AGU PUBLICATIONS

Geophysical Research Letters

RESEARCH LETTER
10.1002/2017GL076319

Key Points:
- The chronology of deep convection is largely random due to the Intrinsic Ocean Variability arising from a mesoscale-eddying ocean
- The spatial patterns of intrinsic variability can be explained by the effect of bottom topography on baroclinic instability
- Our results support the paradigm change from deterministic to probabilistic oceanography

Correspondence to:
R. Waldman,
robin.waldman@meteo.fr

Citation:
Waldman, R., Somot, S., Herrmann, M., Sevault, F., & Isachsen, P. E. (2018). On the chaotic variability of deep convection in the Mediterranean Sea. *Geophysical Research Letters*, *45*. https://doi.org/10.1002/2017GL076319

Received 8 NOV 2017
Accepted 6 FEB 2018
Accepted article online 9 FEB 2018

On the Chaotic Variability of Deep Convection in the Mediterranean Sea

Robin Waldman[1], Samuel Somot[1], Marine Herrmann[2,3], Florence Sevault[1], and Pål Erik Isachsen[4]

[1]Centre National de Recherches Météorologiques (CNRM), Météo-France-CNRS, Toulouse, France, [2]Laboratoire d'Études Géophysiques et d'Océanographie Spatiale (LEGOS), IRD-CNRS-CNES-Université de Toulouse, Toulouse, France, [3]Vietnam Academy of Science and Technology, University of Science and Technology of Hanoi, Hanoi, Vietnam, [4]Geophysical Institute, University of Oslo and Norwegian Meteorological Institute, Oslo, Norway

Abstract Chaotic intrinsic variability is a fundamental driver of the oceanic variability. Its understanding is key to interpret observations, evaluate numerical models, and predict the future ocean and climate. Here we study intrinsic variability of deep convection in the northwestern Mediterranean Sea using an ensemble eddy-resolving hindcast simulation over the period 1979–2013. We find that the variability of deep convection is mostly forced but also, to a considerable extent, intrinsic. The intrinsic variability can dominate the total convection variability locally and over a single winter. It also makes up a significant fraction of its interannual variability but has only modest impacts on the long-term mean state. We find that the occurrence of deep convection is random 18% of years at the basin scale, and 29% locally at the LION observational site. Spatially, the intrinsic variability is highest far from the continental shelf. We relate this pattern to baroclinic instability theory that takes bottom stabilization into account.

1. Introduction

The ocean is a highly turbulent fluid which displays chaotic dynamics from scales of a few centimeters to hundreds of kilometers (Ilicak et al., 2008). The turbulent nature of the flow implies that a large fraction of its variability is unpredictable (Lorenz, 1963). This oceanic "weather" has only recently been characterized in mesoscale-eddying oceanic general circulation models either by imposing a nominal year atmospheric forcing or by performing ensemble simulations with a full atmospheric forcing, both methods giving very similar results (Leroux et al., 2018). This chaotic variability, which we will name Intrinsic Ocean Variability (IOV), was found to play a major role in regulating the temporal variability of ocean characteristics such as its large-scale overturning (Grégorio et al., 2015; Penduff et al., 2014) and horizontal (Penduff et al., 2011; Sérazin et al., 2015, 2016; Venaille et al., 2011) circulation, as well as its heat content (Penduff et al., 2014; Sérazin et al., 2017). The IOV typically dominates the oceanic variability on small spatiotemporal scales (<500 km and $T < 18$ months, Sérazin et al., 2015) but its impacts also extend up to multidecadal (Grégorio et al., 2015) and subbasin scales (>500 km, Sérazin et al., 2015).

Dense water formation (DWF) and oceanic deep convection are a key component of the large-scale thermohaline circulation (Lozier, 2012; Srokosz et al., 2012) and therefore of climate (Buckley & Marshall, 2016; Jackson et al., 2015; Vellinga & Wood, 2002; Winton et al., 2013). Deep convection is localized in a few regions at high latitudes and within semienclosed seas (Marshall & Schott, 1999). The northwestern Mediterranean Sea (NWMed) is one of them, and its proximity to populated coastal areas makes it a well-observed DWF area (Estournel et al., 2016; Leaman & Schott, 1991; MEDOC-Group, 1970; Schott et al., 1996; Testor et al., 2018). Deep convection here forms the Western Mediterranean Deep Waters (WMDW), a water mass filling 69% of the Western Mediterranean Sea volume (Waldman, Somot, et al., 2017) and contributing to form the Mediterranean Outflow Waters which participate in the Global Overturning Circulation (Price et al., 1993). It also modulates the regional circulation (Herrmann et al., 2009; Schroeder et al., 2008), the heat content (Schroeder et al., 2016), and the biogeochemical properties (D'Ortenzio et al., 2014; Herrmann et al., 2014; Santinelli et al., 2013) of the NWMed.

Deep convection in the NWMed is exclusively a winter phenomenon (Marshall & Schott, 1999). It is very intermittent at daily time scales (Waldman, Somot, et al., 2017), but it also shows considerable interannual

variability (Herrmann et al., 2017; Somot et al., 2016) with half of winters being nonconvective. The magnitude of convection itself shows no historical trend (Herrmann et al., 2017) although WMDWs show a warming and saltening trend (Schroeder et al., 2016). The long-term evolution in a changing climate is uncertain, but the highest greenhouse gas emission scenarios project a dramatic reduction of deep convection by 2100 (Adloff et al., 2015). All the aforementioned variability is believed to be dominated by atmospheric forcing (Béranger et al., 2010; Demirov & Pinardi, 2007; Herrmann et al., 2010; L'Hévéder et al., 2013; Sannino et al., 2009; Somot et al., 2016). However, the turbulent mesoscale dynamics, primarily stemming from baroclinic instability, is intrinsic to the ocean itself and can modulate deep convection through the restratification process. The question of how important this IOV is to the total variability of deep convection activity in the NWMed, which has been addressed at the daily time scale by Waldman, Somot, et al. (2017) and Waldman, Herrmann, et al. (2017), remains open at the interannual and climatic time scales, which are the focus of the present work.

Our study uses a multidecadal eddy-resolving ensemble simulation to characterize the IOV of deep convection in the NWMed at the climatological mean, interannual (1980–2013), and daily winter 2013 scales. It also uses baroclinic instability theory to interpret the main spatial patterns of this IOV. The paper is organized as follows: section 2 presents materials and methods, section 3 characterizes the IOV of deep convection for various temporal time scales, section 4 interprets results in the light of baroclinic instability theory, and section 5 summarizes the main results and discusses their implications.

2. Materials and Methods

2.1. NWMED36 Ensemble Simulation

We use the eddy-resolving (2–2.4 km resolution) model NWMED36, which is an AGRIF grid refinement (Debreu et al., 2008; Djath et al., 2014) over the NWMed of the Mediterranean eddy-permitting model NEMOMED12 (Beuvier et al., 2012). NWMED36 has been comprehensively described and validated in terms of DWF on the winter 2013 case study by Waldman, Herrmann, et al. (2017). The numerical configuration used here is identical to this former study except from a partial no-slip lateral momentum boundary condition which ensures more realistic exchanges at Gibraltar Strait. Oceanic convection is parametrized by an enhanced vertical diffusion (10 m^2/s) when static instability occurs.

Here we study the IOV associated with deep convection over the period August 1979 to June 2013 by generating, as did Waldman, Herrmann, et al. (2017), a perturbed 10-member initial state ensemble. The ensemble is designed to realistically represent the observed large-scale hydrography while allowing for an unconstrained chaotic mesoscale. We first run a common 10 year spin-up simulation initialized from the merged Rixen et al. (2005) and MEDAR/MEDATLAS Group (2002) climatologies which represent the Mediterranean hydrography in August 1979 (Hamon et al., 2016; Sevault et al., 2014) and forced similarly as Hamon et al. (2016)'s free run from 1979 to 1989. The large-scale hydrography (running mean of ±50 km) on 1 August 1989 from this simulation is then defined as the common large-scale initial conditions (on 1 August 1979) for the perturbed NWMED36 ensemble. For each of the 10 members we then add to this large-scale field the mesoscale hydrography (residual after withdrawing the running mean of ±50 km) from 1 August of years 1980 to 1989 from the spin-up phase. We then run the ensemble simulation in hindcast mode using the full historical forcing as Hamon et al.'s (2016) free run.

2.2. Diagnostics of Deep Convection

Open-ocean deep convection occurs exclusively when the mixed layer depth (MLD) reaches the top of the WMDW layer (~1,000 m depth, Waldman, Somot, et al., 2017). Here we compute the MLD with the classical $\Delta\rho = 0.01$ kg/m^3 density anomaly criterion with respect to the surface (Somot et al., 2016). We then diagnose the spatial distribution, interannual (1980–2013) and daily variability (winter 2013) of convection. For this one winter season we diagnose daily time series whereas for the interannual variability and climatological mean we diagnose the annual maximum of each parameter, which we will simply refer to as its "annual" value.

The geographic distribution of deep convection will be illustrated with MLD maps. We also produce time series of MLD at the LION site (MLD_{LION}, position shown in Figure 1a) which is a much-studied location within this convection region. We also show time series of the spatial maximum MLD (MLD_{max}) which was previously used to determine the occurrence of convection (Somot et al., 2016). Finally, we diagnose the integrated deep convection volume (V_{MLD}) defined, following Waldman, Somot, et al. (2017), as the volume of mixed layer with MLD > 1,000 m.

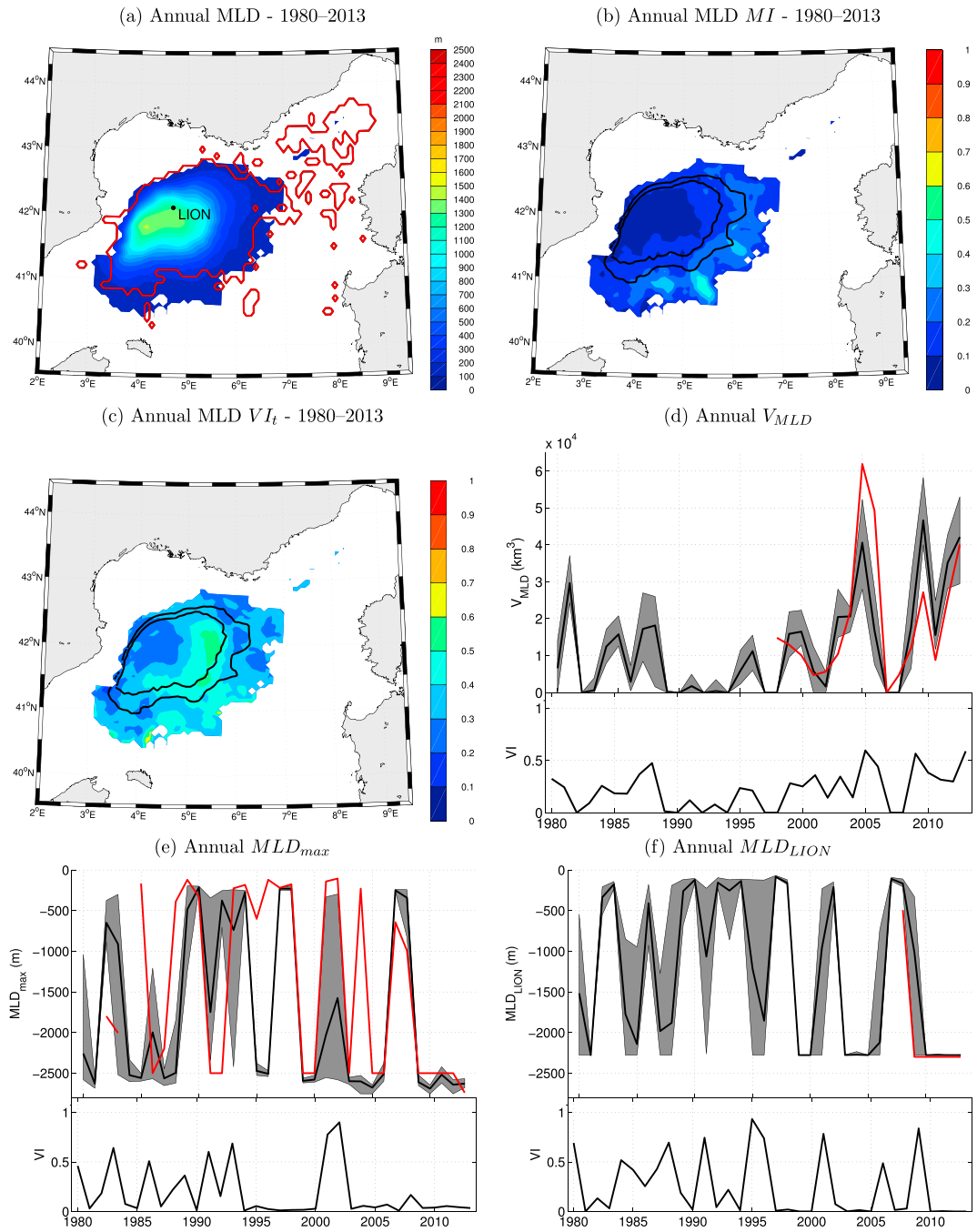

Figure 1. (a) Climatological mean annual mixed layer depth (MLD) in NWMED36 (shades) and observed deep convection areas (MLD > 1,000 m, red contour) in 1980–2013. (b and c) Annual MLD MI (b) and VI_t (c) for 1979–2013. (d–f) Annual deep convection volume (V_{MLD}, d), spatial maximum MLD (MLD_{max}, e), and LION site MLD (MLD_{LION}, f) in NWMED36 (black, ensemble mean and shaded minimum-maximum) and observed (red), and the associated VI. Shaded areas in (a–c) are where deep convection (MLD > 1, 000 m) was simulated by at least one member in the 1980–2013 period and black contours in (b and c) are the ensemble minimum and maximum areas with more than one deep convection day per year.

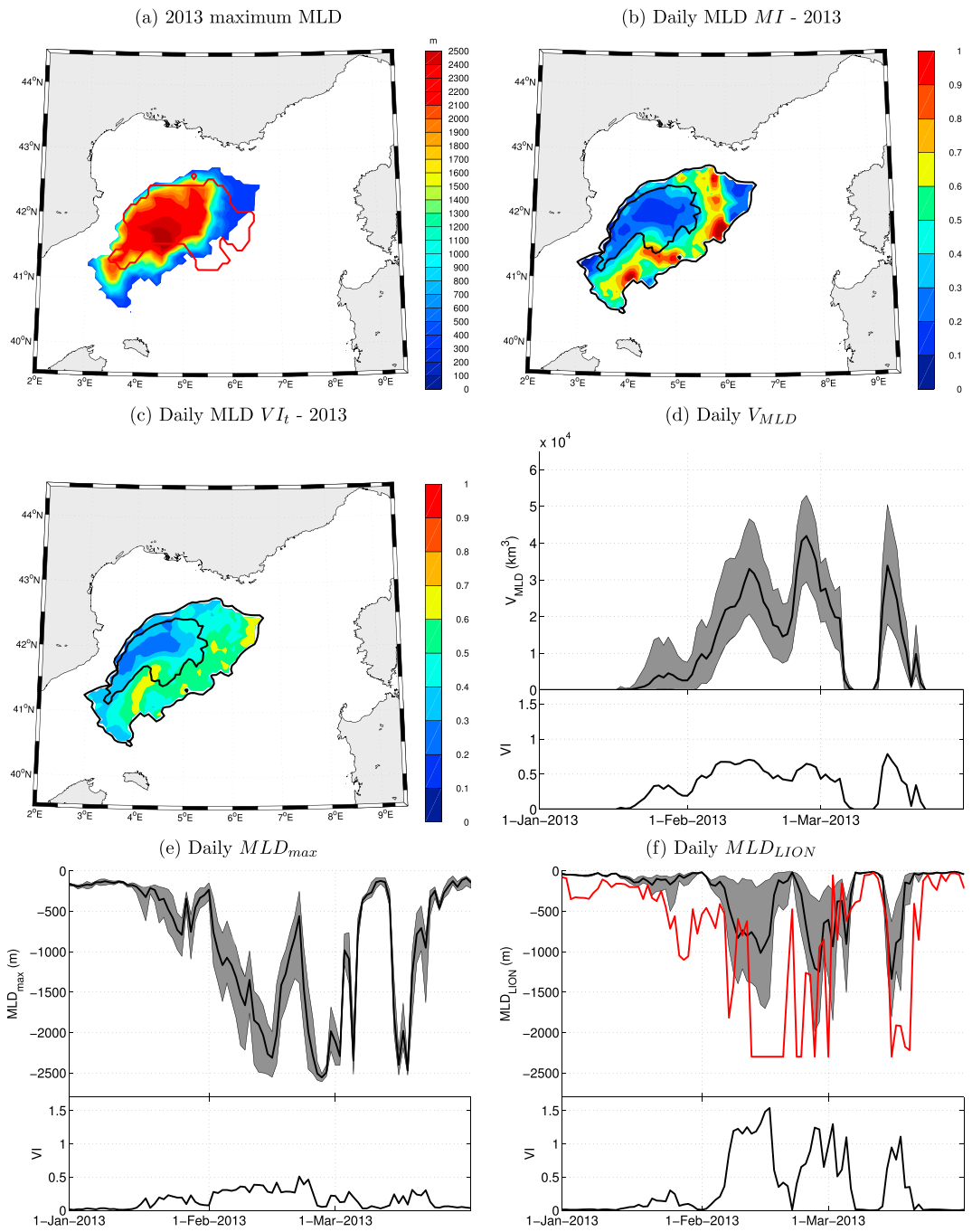

Figure 2. (a) Winter 2013 (January to March) maximum mixed layer depth (MLD) in NWMED36 ensemble mean (shades) and observations (red contour). (b and c) Daily MLD MI (b) and VI_t (c) for winter 2013. (d–f) Daily deep convection volume (V_{MLD}, d), spatial maximum MLD (MLD_{max}, e), and MLD at the LION site (MLD_{LION}, f) in NWMED36 (black, ensemble mean and shaded minimum-maximum) and observed (red), and the associated VI. Shaded areas in (a–c) are where deep convection (MLD > 1,000 m) was simulated by at least one member in 2013 period and black contours in (b and c) are the ensemble minimum and maximum areas with more than one convection day in 2013.

2.3. Observations

We compare the model results with observational indications of deep convection geography, magnitude, and both interannual and winter daily variability. We display the observational estimates of both the 1980–2013 and winter 2013 maximum deep convection areas (Figures 1 and 2, red). For the 1980–2013 period, we construct a map of all locations where DWF was observed by in situ measurements (respectively winters 1987, 1992, and 2013, (Leaman & Schott, 1991; Schott et al., 1996; Waldman, Herrmann, et al., 2017) or by satellite instruments (winters 2007 to 2013, (Houpert et al., 2016)). We extend Houpert et al.'s (2016) estimate of convective activity to the 1998–2006 period using SeaWIFS data and applying their methodology: the annual DWF area is defined as the maximum 8 day mean area with a surface chlorophyll concentration $[Chl_A]_s < 0.15$ mg/m^3. For winter 2013 we show Waldman, Herrmann, et al.'s (2017) maximum DWF area. In terms of magnitude and chronology, we use Herrmann et al.'s (2017) 1998 to 2012 and Waldman, Herrmann, et al.'s (2017) 2013 V_{MLD} estimates. These are based respectively on satellite observations (sea level anomaly and $[Chl_A]_s$) and on in situ MLD measurements. We then use Somot et al.'s (2016) observed annual MLD_{max} to estimate the DWF interannual variability. Finally, we use Houpert et al.'s (2016) MLD_{LION} estimate to obtain its daily winter 2013 variability.

2.4. Statistics of Intrinsic Variability

We quantify the impact of the IOV both on the mean state and on the total temporal variability. Let $X(t, i)$ be a physical parameter at time t and for ensemble member i. $X(t, i)$ can have a spatial dependence (e.g., the MLD) or not (e.g., V_{MLD}). $X(t, i)$ can be written as

$$X(t,i) = m_i(X(t,i)) + (X(t,i) - m_i(X(t,i))) \tag{1}$$

with m_i the ensemble mean. By construction, $m_i(X(t, i))$ represents the forced and $(X(t, i) - m_i(X(t, i)))$ the intrinsic component of $X(t, i)$.

We quantify the impact of the IOV on the mean state as

$$\mathrm{MI} = \frac{\sigma_i(m_t(X(t,i)))}{m_i(m_t(X(t,i)))} \tag{2}$$

with m_t, m_i, σ_t, and σ_i the temporal and ensemble mean and standard deviations. MI is thus the relative intrinsic variability of the mean state.

We then quantify the intrinsic contribution to the total temporal variability as

$$\mathrm{VI}(t) = \frac{\sigma_i(X(t,i))}{\sqrt{m_i(\sigma_t(X)^2)}} \tag{3}$$

which is the ratio between the time-dependent intrinsic variability and the total temporal variability. Its temporal mean and temporal mean squared values are $\mathrm{VI}_t = m_t(\mathrm{VI}(t))$ and $\mathrm{VI}_t^2 = m_t(\mathrm{VI}(t)^2)$. Assuming $m_t(X(t, i))$ is identical between all members, then VI_t^2 is the fraction of total variance explained by IOV, the remaining $1 - \mathrm{VI}_t^2$ being the forced variance (Sérazin et al., 2017). Whereas VI_t^2 is between 0 and 1, $\mathrm{VI}(t)$ can exceed 1 over specific periods.

3. Intrinsic Variability of Oceanic Deep Convection

3.1. Model Evaluation

The climatological mean (mean over years 1980–2013) annual MLD (Figure 1a) reveals that deep convection occurs in NWMED36 primarily off the Gulf of Lions in an open-sea area centered close to the LION site. The model is in good agreement with observations although it underestimates the occurrence of deep convection in the Ligurian Sea to the northeast. For the specific winter of 2013 (Figure 2a), the simulated and observed DWF patterns are also in good agreement.

The annual V_{MLD}, MLD_{max}, and MLD_{LION} (Figures 1d–1f) reveal the strong interannual variability of deep convection. In both NWMED36 and observations, most winters have either no deep convection ($MLD_{max} < 1{,}000$ m) or deep convection that reaches the ocean bed ($MLD_{max} > 2{,}000$ m). This is consistent with most of the NWMed stratification being localized in the 0–200 m depth layer (Waldman, Somot, et al., 2017). DWF is more frequent in NWMED36 (68%) than in the observations (52%), which could also result from observation undersampling issues. The modeled annual V_{MLD} closely follows the observed chronology

Table 1
Intrinsic Variability of the Deep Convection Volume (V_{MLD}), LION Site MLD (MLD_{LION}), and the Spatial Maximum MLD (MLD_{max}) at the Climatological Mean, Interannual, and Winter 2013 Scales

Parameter	Climatological mean (MI)	Interannual variability (VI_t and VI_t^2)	Winter 2013 mean (MI)	Winter 2013 daily variability (VI_t and VI_t^2)
V_{MLD}	7%	22% and 8%	30%	27% and 14%
MLD_{max}	3%	19% and 10%	10%	16% and 4%
MLD_{LION}	6%	25% and 16%	36%	35% and 33%

(correlation $r = 0.71$) and shows only a very weak mean bias (+950 km^3). We take this as confirmation that NWMED36 realistically represents the chronology and mean magnitude of convection.

During the winter of 2013 the observed daily MLD_{LION} (Figure 2f) shows several intermittent DWF events which are also simulated by NWMED36. The model typically underestimates the maximum MLD reached. Waldman, Somot, et al. (2017) related this to a southward bias in the location of the buoyant Northern Current. But, all over, the NWMED36 fields are realistic in a wide range of aspects and time scales.

3.2. Intrinsic Variability of the Climatological Mean State

Figure 1b displays the annual MLD's MI map which determines whether the IOV impacts the mean location of DWF in the 1980–2013 period. MI is lower than 10% (0.1) over most of the area where all NWMED36 members simulate more than 1 day of DWF per year (inner black contour), whereas it can be larger than 30% over areas where DWF occurs less than 1 day per year in all members (outside the outer black contour). This means that IOV only marginally impacts the climatological mean geography of convection except in peripherical areas where DWF occurs very seldom. Spatially, both the annual mean frequency of DWF (black contours) and its location (shades) have the highest IOV to the southeast and the lowest to the northwest. Table 1 displays the mean statistics of IOV. Consistent with the result for the annual MLD we also find a low MI for the annual V_{MLD} (7%), MLD_{max} (3%) and MLD_{LION} (6%). So we conclude that on the climatological average, deep convection is barely impacted by IOV, except along the southeastern edge of the active region.

3.3. Intrinsic Interannual Variability During 1980–2013

Figure 1c displays the annual MLD's VI_t map during 1980–2013 which determines where the IOV significantly contributes to the interannual variability of convection. VI_t is larger than 30% over most of the simulated DWF area, both at locations where DWF is frequent (inner black contour) and rare (outside the outer black contour). Again, the intrinsic variability is highest to the southeast and lowest to the northwest. The annual V_{MLD} and MLD_{max} (Figures 1d and 1e) reveal that the occurrence or not of DWF is IOV dependent (DWF occurs in at least one member but not all) in 18% of winters, and when diagnosed locally (MLD_{LION}, Figure 1f), this dependency increases to 29%. The IOV is hence a major driver for the timing of deep convection at interannual time scales. It is highly variable in time (VI between 0 and 90%) and dependent on the parameter considered. In particular, IOV has its largest impact on MLD_{max} during weak convective winters and on V_{MLD} during intense convective winters. The interannual VI_t in the 1980–2013 period takes on mean values of 22%, 19%, and 25% for V_{MLD}, MLD_{max} and MLD_{LION} (Table 1). And VI_t^2, the intrinsic fraction of the total temporal variance, is 8%, 10%, and 16% for V_{MLD}, MLD_{max}, and MLD_{LION}. This confirms that deep convection is mostly forced, as expected, but that IOV is still a significant contribution to its interannual variability, especially to the southeast of the DWF area.

3.4. Intrinsic High-Frequency Variability During the 2013 Winter

The above results show that the intrinsic variability of V_{MLD} (the variable most likely to be connected with the larger-scale thermohaline circulation) is highest during intense convective winters. We therefore now focus on the well-observed 2013 winter (January to March) in which convection activity was intense. Both the MI and VI_t of MLD this winter exceed 40% over most of the simulated DWF area (Figures 2b and 2c), mainly where IOV determines the occurrence or not of DWF (between both black contours). Hence, the daily variability of deep convection can locally be mostly chaotic. Consistent with our findings for longer time scales, IOV is highest to the southeast and lowest to the northwest. For this winter season MI for variables V_{MLD}, MLD_{max}, and MLD_{LION} is 30%, 10%, and 36% (Table 1), showing that IOV significantly modulates the mean magnitude of convection. VI_t for the same variables is 27%, 16%, and 35% and VI_t^2; the IOV fraction of the total variance is 14%, 4%, and 33%. Hence, the winter variance of deep convection is also mostly forced, but its intrinsic part is significant, especially when diagnosed locally at the LION site.

Finally, the daily IOV signal (Figures 2d–2f) differs highly when deep convection is diagnosed globally (V_{MLD} and MLD_{max}) or locally (MLD_{LION}). It lies below 50% at all times for MLD_{max} but can exceed 50% for V_{MLD} and can even exceed 100% for MLD_{LION}. Locally at LION, all the simulated convection periods in winter 2013 are IOV dependent (at least one member does not simulate convection, Figure 2f). This confirms that also at the winter scale, IOV is a major driver for the timing of deep convection which is hence largely random locally. We conclude that IOV has a significant impact both on the mean state and daily variability during this intense convective winter, especially when diagnosed locally and again to the southeastern edge. As such, our results confirm those found by Waldman, Somot, et al. (2017) and Waldman, Herrmann, et al. (2017) in their 2012–2013 case study.

4. Baroclinic Instability as a Source of Intrinsic Variability

The above results indicate that intrinsic variability of deep convection in the NWMed displays a fairly robust spatial pattern, being lowest in the northwest, in the vicinity of the continental shelf, and highest to the south and southeast, far from the shelf. In NWMED36, the sources of intrinsic chaotic variability are the resolved macroturbulent scales, that is, eddy stirring stemming primarily from barotropic and baroclinic instability. As it turns out, the root mean square (RMS) of modeled sea surface height anomaly (SSH), a diagnostic which has been proposed to reflect eddy diffusivities (Holloway, 1986; Isachsen & Nøst, 2012), is highest in the southern NWMed (Figure 3a). Hence, a plausible hypothesis is that the observed IOV stems from a modulation of the background stratification by the eddy field. But which instability process is responsible? The region-averaged barotropic and baroclinic conversion rates (Saenko et al., 2014), computed over the upper 1,000 m for 1980–2012 from one ensemble member, reach respectively -4.7×10^{-11} m^2/s^3 and $+9.3 \times 10^{-10}$ m^2/s^3. The dominating (and positive) baroclinic conversion suggests that baroclinic instability is the main source of eddy activity in the NWMed. We therefore aim at interpreting the spatial patterns of IOV in the light of elementary baroclinic instability theory.

Eady theory (Eady, 1949) gives, in a highly idealized framework, useful analytical predictions regarding baroclinic instability. We follow Stone's (1972) formalism by computing an eddy diffusivity κ_t from the growth rate ω and wave number μ of the most unstable Eady waves. It gives an estimate of the transport capacity of mesoscale turbulence, which modulates the restratification and therefore can impact convection. Eady theory predicts

$$\omega = 0.31 \frac{f}{\bar{N}} \overline{|\partial_z \mathbf{u_g}|} \tag{4}$$

and

$$\mu = 1.61 \frac{f}{\bar{N} H} \tag{5}$$

with f the Coriolis parameter, $\bar{N} = \overline{\sqrt{-\frac{g}{\rho_0}\partial_z \rho}}$ the vertical-mean Brunt-Väisälä frequency, g the gravity acceleration, ρ_0 and ρ the reference and potential densities, $\overline{|\partial_z \mathbf{u_g}|} = \frac{g}{\rho_0 f} \overline{|\nabla_h \rho|}$ the vertical-mean vertical geostrophic current shear and H the bottom depth. The vertical means are taken over the top 1,000 m to limit errors from thermobaricity. Hence, the Eady eddy diffusivity is

$$\kappa_t = \frac{\omega}{\mu^2} = 0.12 \frac{H^2}{f^2} \left(\frac{g}{\rho_0}\right)^{3/2} \overline{|\nabla_h \rho|} \overline{\sqrt{\partial_z \rho}} \tag{6}$$

So the internal oceanic parameters that determine κ_t are the horizontal and vertical density stratifications. We extract these from NWMED36's ensemble winter mean (January to March) hydrography over the 1980–2013 period.

The calculated κ_t (Figure 3b) exceeds 100 m^2/s over most of the open-sea domain. It is maximum to the south of the NWMed and around the cyclonic gyre surrounding the DWF region. To the northwest, the large diffusivities are due to high Eady growth rates, whereas to the south, they are driven by large wavelengths (not shown). However, this pattern would suggest a large IOV along all boundaries of the DWF area, including to the northwest. This, as shown above, is not the case.

Here we test the additional hypothesis that baroclinic instability in the NWMed is affected by the large-scale bathymetric slope. As illustrated in Figure 3c, topographic beta ($|\beta_t| = \frac{f}{H}|\nabla H|$) exceeds planetary beta in the NWMed by orders of magnitude. This topographic potential vorticity gradient is also stronger along the

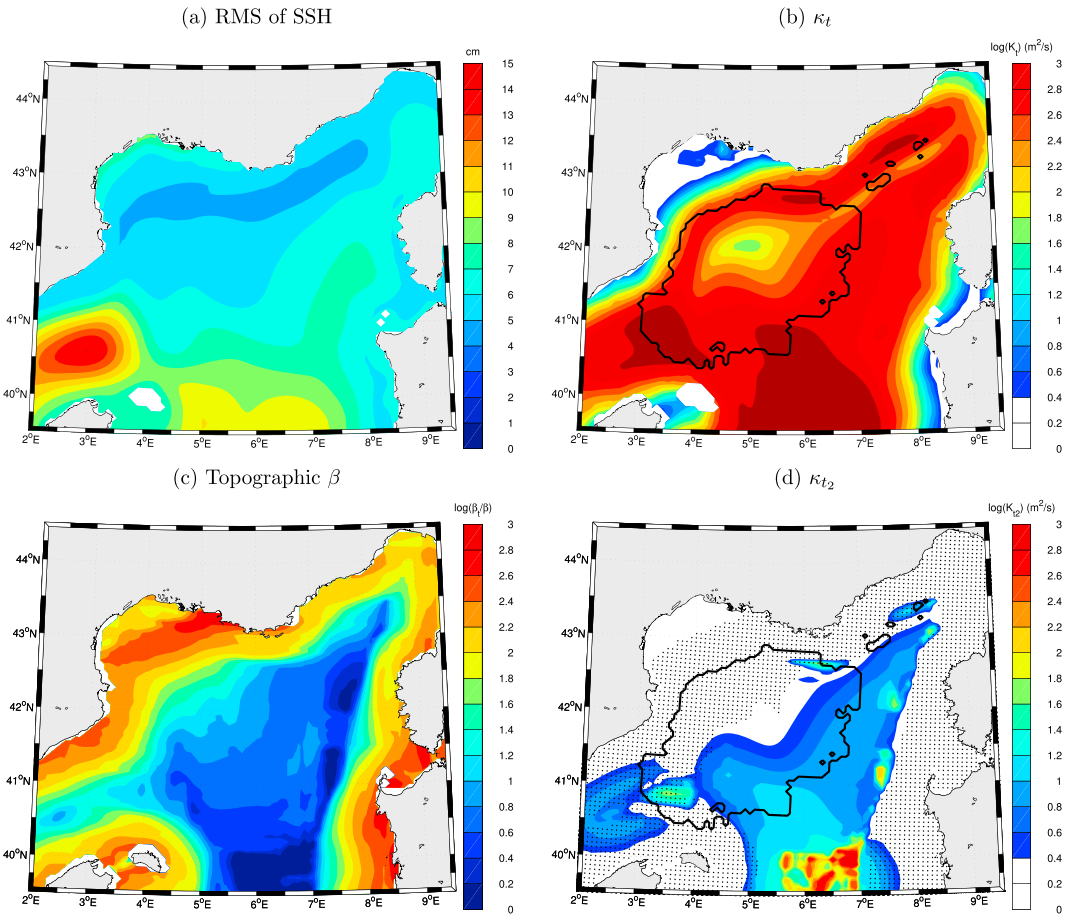

Figure 3. (a) RMS of modeled sea surface height anomaly (SSH) over the 1979–2013 period, (b) wintertime (JFM) eddy diffusivity predicted from flat-bottom Eady theory (note the logarithmic color scales), (c) the topographic potential vorticity gradient nondimensionalized by planetary beta, and (d) eddy diffusivity from topographically aware Eady theory (Blumsack & Gierasch, 1972). Black contours in (b and d) show where deep convection was simulated at least 1 day in the 1979–2013 period, and black dots in (d) show regions having bottom slope $|\nabla H| > 0.005$.

continental slope in the north and weaker toward the south, roughly tracing out the modeled patterns of SSH variability. Blumsack and Gierasch (1972) added the effect of a sloping bottom to the Eady model and found that the key regulator of growth is a bottom topography parameter δ which measures the ratio between the bathymetric and isopycnal slopes:

$$\delta = \frac{|\nabla H|^2}{\bar{\mathbf{s}} \cdot \nabla H}, \quad \bar{\mathbf{s}} = -\frac{\overline{\nabla_h \rho}}{\overline{\partial_z \rho}}. \tag{7}$$

In the modified Eady model the isopycnal slope **s** is constant, but for a realistic application, like ours, a vertical mean must be taken (hence the overbars in the expression). Blumsack and Gierasch's theory predicts an overall suppression of baroclinic instability by the bathymetry slope but actually fastest growth for $\delta = 0.5$. Isachsen (2011) tested the theory in idealized primitive equation simulations and found good agreement for $\delta < 0$. However, he found that diagnosed eddy diffusivities (normalized by the flat-bottom Eady prediction) were maximum for $\delta = 0$ (flat bottom) and then decayed approximately exponentially before flattening out for $\delta > 1$. Here we fit empirical functions of δ to his modeling results (his Figure 9) as follows:

$$\delta < 0, \quad \kappa_{t_2} = 0.59\,10^{-0.59|\delta|} \times \kappa_t \tag{8}$$

$$0 < \delta < 1, \quad \kappa_{t_2} = 0.59\,10^{-2.0|\delta|} \times \kappa_t \tag{9}$$

$$\delta > 1, \quad \kappa_{t_2} = 0.59\,10^{-2.0} \times \kappa_t \tag{10}$$

Applying these expressions to the NWMed suggests that κ_{t_2} is everywhere lower than the prediction from flat-bottom Eady theory (Figure 3d). The magnitude of the suppression is likely overestimated, as discussed by Isachsen (2015), but the qualitative effect is consistent with the notion of eddy transport being inhibited by topographic potential vorticity gradients. We now identify a strong spatial pattern, with κ_{t_2} being lowest to the northwest and highest to the southeast. This is caused by the bathymetry slope decaying with increasing distance from the shelf. The areas with strongest predicted κ_{t_2} are now in better agreement with the pattern of SSH variability and high-IOV areas previously identified. Largest predicted diffusivities are found in a near flat-bottom area to the south of the NWMed, outside of the active convection region. But the elevated values extend up to the regions where convection displays a high intrinsic variability. We, hence, take these results as support for the hypothesis that deep convection IOV is mostly generated through baroclinic instability of the cyclonic gyre and that this process is likely suppressed in the northwest by the continental bank slope.

5. Conclusions

In this study, we have characterized and physically interpreted the IOV of DWF in the NWMed. For that we have performed an ensemble eddy-resolving hindcast simulation over the period 1979–2013 with a perturbed initial state at the mesoscale. The simulations are realistic in a wide range of aspects and time scales of DWF. We have quantified the IOV from the ensemble spread in the properties of convection. At the climatological mean scale, DWF displays a low IOV. But at interannual time scales IOV is a significant contribution to DWF variability. And during the winter of 2013, IOV modulates and can locally dominate the mean magnitude as well as the daily variability of deep convection. At both interannual and daily time scales, the chronology of deep convection is to a large extent random. In particular, intrinsic variability determines the occurrence or not of deep convection 18% of years at the basin scale and 29% locally at the LION observational site. We also found that at all time scales the IOV is highest to the southeast of the deep convection area. To interpret this pattern, we plotted eddy diffusivity maps based on simplified baroclinic instability theory that takes topographic slope suppression into account. Our results support that intrinsic variability of deep convection is mostly generated through baroclinic instability of the cyclonic gyre but that this process is suppressed in the northwest by the bathymetric slope.

On a more general level, we note that the intrinsic chaotic fraction of the DWF signal is neither predictable nor reproductible (Lorenz, 1963). Therefore, we advocate for a paradigm change in the analysis of numerical simulations to ensure the robustness of results in light of intrinsic variability. First, model evaluation should be reduced to the nonintrinsic part of the signal. Hence, care should be made when using observations, especially local and/or high frequency, to constrain numerical models. In particular, we have shown that the chronology of convection at the LION reference site is to a large extent random. Second, physical sensitivity studies showing a low impact on highly intrinsic phenomena are likely to be insignificant. We therefore recommend at least to acknowledge the intrinsic variability in deterministic (one member) modeling approaches or at best to adopt probabilistic (ensemble) approaches that account for it. Finally, both the intrinsic variability and the control of eddy fluxes by bathymetry are relevant for climate. Their parametrization in low-resolution models is hence highly needed: the former shows promising results (Brankart et al., 2015; Williams et al., 2016) whereas the latter has proven to be challenging (Isachsen, 2015).

Acknowledgments
We would like to thank Michael Spall for the helpful discussion on the control of eddy fluxes by the bathymetry slope, and Thierry Penduff and Stephanie Leroux for interactions on the metrics of intrinsic variability. We also thank two anonymous reviewers for the useful remarks. This work is a contribution to the HyMeX program (*HYdrological cycle in the Mediterranean EXperiment*-https://www.hymex.org) through INSU-MISTRALS support. This work is part of the Flagship Pilot Study on Air-Sea Coupling within the Med-CORDEX initiative (https://www.medcordex.eu). Observations used in this study are from cited references, and model outputs are publicly available at http://mistrals.sedoo.fr/?editDatsId=1494&datsId=1494&project_name=HyMeX can be made available upon request by contacting robin.waldman@meteo.fr.

References

Adloff, F., Somot, S., Sevault, F., Jordà, G., Aznar, R., Déqué, M., et al. (2015). Mediterranean Sea response to climate change in an ensemble of twenty first century scenarios. *Climate Dynamics*, *45*(9–10), 2775–2802.

Béranger, K., Drillet, Y., Houssais, M.-N., Testor, P., Bourdallé-Badie, R., Alhammoud, B., et al. (2010). Impact of the spatial distribution of the atmospheric forcing on water mass formation in the Mediterranean Sea. *Journal of Geophysical Research*, *115*, C12041. https://doi.org/10.1029/2009JC005648

Beuvier, J., Béranger, K., Brossier, C. L., Somot, S., Sevault, F., Drillet, Y., et al. (2012). Spreading of the Western Mediterranean Deep Water after winter 2005: Time scales and deep cyclone transport. *Journal of Geophysical Research*, *117*, C07022. https://doi.org/10.1029/2011JC007679

Blumsack, S. L., & Gierasch, P. (1972). Mars: The effects of topography on baroclinic instability. *Journal of the Atmospheric Sciences*, *29*(6), 1081–1089.

Brankart, J.-M., Candille, G., Garnier, F., Calone, C., Melet, A., Bouttier, P.-A., et al. (2015). A generic approach to explicit simulation of uncertainty in the NEMO ocean model. *Geoscientific Model Development*, *8*(5), 1285–1297. https://doi.org/10.5194/gmd-8-1285-2015

Buckley, M. W., & Marshall, J. (2016). Observations, inferences, and mechanisms of the Atlantic Meridional Overturning Circulation: A review. *Reviews of Geophysics*, *54*, 5–63. https://doi.org/10.1002/2015RG000493

Debreu, L., Vouland, C., & Blayo, E. (2008). AGRIF: Adaptive grid refinement in Fortran. *Computers and Geosciences*, *34*(1), 8–13. https://doi.org/10.1016/j.cageo.2007.01.009

Demirov, E. K., & Pinardi, N. (2007). On the relationship between the water mass pathways and eddy variability in the Western Mediterranean Sea. *Journal of Geophysical Research*, *112*, C02024. https://doi.org/10.1029/2005JC003174

Djath, N., Melet, A., Verron, J., Molines, J.-M., Barnier, B., Gourdeau, L., & Debreu, L. (2014). A 1/36 degrees model of the Solomon Sea embedded into a global ocean model: On the setting up of an interactive open boundary nested model system. *Journal of Operational Oceanography*, *7*, 34–46. https://doi.org/10.1080/1755876X.2014.11020151

D'Ortenzio, F., Lavigne, H., Besson, F., Claustre, H., Coppola, L., Garcia, N., et al. (2014). Observing mixed layer depth, nitrate and chlorophyll concentrations in the northwestern Mediterranean: A combined satellite and NO_3 profiling floats experiment. *Geophysical Research Letters*, *41*, 6443–6451. https://doi.org/10.1002/2014GL061020

Eady, E. T. (1949). Long waves and cyclone waves. *Tellus*, *1*(3), 33–52. https://doi.org/10.1111/j. 2153-3490.1949.tb01265.x

Estournel, C., Testor, P., Taupier-Letage, I., Bouin, M., Coppola, L., Durand, P., et al. (2016). HyMeX-SOP2, the field campaign dedicated to dense water formation in the north-western Mediterranean. *Oceanography*, *29*, 196–206. https://doi.org/10.5670/oceanog.2016.94

Grégorio, S., Penduff, T., Sérazin, G., Molines, J.-M., Barnier, B., & Hirschi, J. (2015). Intrinsic variability of the Atlantic Meridional Overturning Circulation at interannual-to-multidecadal time scales. *Journal of Physical Oceanography*, *45*(7), 1929–1946.

Hamon, M., Beuvier, J., Somot, S., Lellouche, J.-M., Greiner, E., Jordà, G., et al. (2016). Design and validation of MEDRYS, a Mediterranean Sea reanalysis over the period 1992–2013. *Ocean Science*, *12*(2), 577–599. https://doi.org/10.5194/os-12-577-2016

Herrmann, M., Auger, P.-A., Ulses, C., & Estournel, C. (2017). Long-term monitoring of ocean deep convection using multisensors altimetry and ocean color satellite data. *Journal of Geophysical Research: Oceans*, *122*, 1457–1475. https://doi.org/10.1002/2016JC011833

Herrmann, M., Bouffard, J., & Béranger, K. (2009). Monitoring open-ocean deep convection from space. *Geophysical Research Letters*, *36*, L03606. https://doi.org/10.1029/2008GL036422

Herrmann, M., Estournel, C., Diaz, F., & Adloff, F. (2014). Impact of climate change on the Northwestern Mediterranean Sea pelagic planktonic ecosystem and associated carbon cycle. *Journal of Geophysical Research: Oceans*, *119*, 5815–5836. https://doi.org/10.1002/2014JC010016

Herrmann, M., Sevault, F., Beuvier, J., & Somot, S. (2010). What induced the exceptional 2005 convection event in the northwestern Mediterranean basin? Answers from a modeling study. *Journal of Geophysical Research*, *115*, C12051. https://doi.org/10.1029/2010JC006162

Holloway, G. (1986). Estimation of oceanic eddy transports from satellite altimetry. *Nature*, *323*, 243–244. https://doi.org/10.1038/323243a0

Houpert, L., Durrieu de Madron, X., Testor, P., Bosse, A., D'Ortenzio, F., Bouin, M., et al. (2016). Observations of open-ocean deep convection in the northwestern Mediterranean Sea: Seasonal and interannual variability of mixing and deep water masses for the 2007–2013 period. *Journal of Geophysical Research: Oceans*, *121*, 8139–8171. https://doi.org/10.1002/2016JC011857

Ilicak, M., Ozgokmen, T. M., Peters, H., Baumert, H. Z., & Iskandarani, M. (2008). Very large eddy simulation of the red sea overflow. *Ocean Modelling*, *20*(2), 183–206. https://doi.org/10.1016/j.ocemod.2007.08.002

Isachsen, P. E. (2011). Baroclinic instability and eddy tracer transport across sloping bottom topography: How well does a modified Eady model do in primitive equation simulations? *Ocean Modelling*, *39*(1–2), 183–199. https://doi.org/10.1016/j.ocemod.2010.09.007

Isachsen, P. E. (2015). Baroclinic instability and the mesoscale eddy field around the Lofoten Basin. *Journal of Geophysical Research: Oceans*, *120*, 2884–2903. https://doi.org/10.1002/2014JC010448

Isachsen, P. E., & Nøst, O. A. (2012). The air-sea transformation and residual overturning circulation within the Nordic Seas. *Journal of Marine Research*, *70*(1), 31–68. https://doi.org/10.1357/002224012800502372

Jackson, L. C., Kahana, R., Graham, T., Ringer, M. A., Woollings, T., Mecking, J. V., & Wood, R. A. (2015). Global and European climate impacts of a slowdown of the AMOC in a high resolution GCM. *Climate Dynamics*, *45*(11), 3299–3316. https://doi.org/10.1007/s00382-015-2540-2

Leaman, K. D., & Schott, F. (1991). Hydrographic structure of the convection regime in the Gulf of Lions: Winter 1987. *Journal of Physical Oceanography*, *21*, 575–597.

Leroux, S., Penduff, T., Bessieres, L., Molines, J.-M., Brankart, J.-M., Serazin, G., et al. (2018). Intrinsic and atmospherically-forced variability of the AMOC: Insights from a large ensemble ocean hindcast. *Journal of Climate*, *31*, 1183–1203. https://doi.org/10.1175/JCLI-D-17-0168.1

L'Hévéder, B., Li, L., Sevault, F., & Somot, S. (2013). Interannual variability of deep convection in the Northwestern Mediterranean simulated with a coupled AORCM. *Climate Dynamics*, *41*(3–4), 937–960. https://doi.org/10.1007/s00382-012-1527-5

Lorenz, E. N. (1963). Deterministic nonperiodic flow. *Journal of the Atmospheric Sciences*, *20*(2), 130–141.

Lozier, M. S. (2012). Overturning in the North Atlantic. *Annual review of marine science*, *4*, 291–315.

Marshall, J., & Schott, F. (1999). Open-ocean convection: Observations, theory, and models. *Reviews of Geophysics*, *37*(1), 1–64.

MEDAR/MEDATLAS Group (2002). MEDAR/MEDATLAS 2002 database. Cruise inventory, observed and analysed data of temperature and bio-chemical parameters, 4 CDrom.

MEDOC-Group (1970). Observations of formation of deep-water in the Mediterranean Sea. *Nature*, *227*, 1037–1040.

Penduff, T., Barnier, B., Terray, L., Bessières, L., Sérazin, G., Gregorio, S., et al. (2014). Ensembles of eddying ocean simulations for climate (p. 26). CLIVAR WGOMD Workshop on high.

Penduff, T., Juza, M., Barnier, B., Zika, J., Dewar, W. K., Treguier, A.-M., et al. (2011). Sea level expression of intrinsic and forced ocean variabilities at interannual time scales. *Journal of Climate*, *24*(21), 5652–5670.

Price, J. F., Baringer, M. O., Lueck, R. G., Johnson, G. C., Ambar, I., Parrilla, G., et al. (1993). Mediterranean outflow mixing and dynamics. *Science*, *259*(5099), 1277–1282. https://doi.org/10.1126/science.259.5099.1277

Rixen, M., Beckers, J.-M., Levitus, S., Antonov, J., Boyer, T., Maillard, C., et al. (2005). The western Mediterranean deep water: A proxy for climate change. *Geophysical Research Letters*, *32*, L12608. https://doi.org/10.1029/2005GL022702

Saenko, O. A., Dupont, F., Yang, D., Myers, P. G., Yashayaev, I., & Smith, G. C. (2014). Role of resolved and parameterized eddies in the Labrador Sea balance of heat and buoyancy. *Journal of Physical Oceanography*, *44*(12), 3008–3032.

Sannino, G., Herrmann, M., Carillo, A., Rupolo, V., Ruggiero, V., Artale, V., & Heimbach, P. (2009). An eddy-permitting model of the Mediterranean Sea with a two-way grid refinement at the Strait of Gibraltar. *Ocean Modelling*, *30*(1), 56–72. https://doi.org/10.1016/j.ocemod.2009.06.002

Santinelli, C., Hansell, D. A., & Ribera d'Alcalà, M. (2013). Influence of stratification on marine dissolved organic carbon (DOC) dynamics: The Mediterranean Sea case. *Progress in Oceanography*, *119*, 68–77.

Schott, F., Visbeck, M., Send, U., Fisher, J., Stramma, L., & Desaubies, Y. (1996). Observations of deep convection in the Gulf of Lions, northern Mediterranean, during the winter of 1991/1992. *Journal of Physical Oceanography*, *26*, 505–524.

Schroeder, K., Chiggiato, J., Bryden, H., Borghini, M., & Ismail, S. B. (2016). Abrupt climate shift in the western Mediterranean Sea. *Scientific Reports*, *6*, 23009. https://doi.org/10.1038/srep23009

Schroeder, K., Ribotti, A., Borghini, M., Sorgente, R., Perilli, A., & Gasparini, G. P. (2008). An extensive western Mediterranean deep water renewal between 2004 and 2006. *Geophysical Research Letters*, *35*, L18605. https://doi.org/10.1029/2008GL035146

Sérazin, G., Meyssignac, B., Penduff, T., Terray, L., Barnier, B., & Molines, J.-M. (2016). Quantifying uncertainties on regional sea level change induced by multidecadal intrinsic oceanic variability. *Geophysical Research Letters*, *43*, 8151–8159. https://doi.org/10.1002/2016GL069273

Sérazin, G., Jaymond, A., Leroux, S., Penduff, T., Bessières, L., Llovel, W., et al. (2017). A global probabilistic study of the ocean heat content low-frequency variability: Atmospheric forcing versus oceanic chaos. *Geophysical Research Letters*, *44*, 5580–5589. https://doi.org/10.1002/2017GL073026

Sérazin, G., Penduff, T., Grégorio, S., Barnier, B., Molines, J.-M., & Terray, L. (2015). Intrinsic variability of sea level from global ocean simulations: Spatiotemporal scales. *Journal of Climate*, *28*(10), 4279–4292.

Sevault, F., Somot, S., Alias, A., Dubois, C., Lebeaupin-Brossier, C., Nabat, P., et al. (2014). A fully coupled Mediterranean regional climate system model: Design and evaluation of the ocean component for the 1980–2012 period. *Tellus A: Dynamic Meteorology and Oceanography*, *66*(1). https://doi.org/10.3402/tellusa.v66.23967

Somot, S., Houpert, L., Sevault, F., Testor, P., Bosse, A., Taupier-Letage, I., et al. (2016). Characterizing, modelling and understanding the climate variability of the deep water formation in the North-Western Mediterranean Sea. *Climate Dynamics*. https://doi.org/10.1007/s00382-016-3295-0

Srokosz, M., Baringer, M., Bryden, H., Cunningham, S., Delworth, T., Lozier, S., et al. (2012). Past, present, and future changes in the atlantic meridional overturning circulation. *Bulletin of the American Meteorological Society*, *93*(11), 1663–1676.

Stone, P. H. (1972). A simplified radiative-dynamical model for the static stability of rotating atmospheres. *Journal of the Atmospheric Sciences*, *29*(3), 405–418. https://doi.org/10.1175/1520-0469(1972)029<0405:ASRDMF>2.0.CO;2

Testor, P., Bosse, A., Houpert, L., Margirier, F., Mortier, L., Legoff, H., et al. (2018). Multiscale observations of deep convection in the northwestern Mediterranean Sea during winter 2012–2013 using multiple platforms. *Journal of Geophysical Research: Oceans*, *123*. https://doi.org/10.1002/2016JC012671

Vellinga, M., & Wood, R. A. (2002). Global climatic impacts of a collapse of the atlantic thermohaline circulation. *Climatic Change*, *54*(3), 251–267. https://doi.org/10.1023/A:1016168827653

Venaille, A., Le Sommer, J., Molines, J.-M., & Barnier, B. (2011). Stochastic variability of oceanic flows above topography anomalies. *Geophysical Research Letters*, *38*, L16611. https://doi.org/10.1029/2011GL048401

Waldman, R., Herrmann, M., Somot, S., Arsouze, T., Benshila, R., Bosse, A., et al. (2017). Impact of the mesoscale dynamics on ocean deep convection: The 2012–2013 case study in the northwestern Mediterranean Sea. *Journal of Geophysical Research: Oceans*, *122*, 8813–8840. https://doi.org/10.1002/2016JC012587

Waldman, R., Somot, S., Herrmann, M., Bosse, A., Caniaux, G., Estournel, C., et al. (2017). Modeling the intense 2012–2013 dense water formation event in the northwestern Mediterranean Sea: Evaluation with an ensemble simulation approach. *Journal of Geophysical Research: Oceans*, *122*, 1297–1324. https://doi.org/10.1002/2016JC012437

Williams, P. D., Howe, N. J., Gregory, J. M., Smith, R. S., & Joshi, M. M. (2016). Improved climate simulations through a stochastic parameterization of ocean eddies. *Journal of Climate*, *29*(24), 8763–8781. https://doi.org/10.1175/JCLI-D-15-0746.1

Winton, M., Griffies, S. M., Samuels, B. L., Sarmiento, J. L., & Frolicher, T. L. (2013). Connecting changing ocean circulation with changing climate. *Journal Climate*, *26*, 2268–2278.